Preparation of Cd/Pb Chalcogenide Heterostructured Janus Particles *via* Controllable Cation Exchange

Jianbing Zhang,[†,‡] Boris D. Chernomordik,[‡] Ryan W. Crisp,[‡,§] Daniel M. Kroupa,[‡,∥] Joseph M. Luther,[‡] Elisa M. Miller,[‡] Jianbo Gao,[⊥] and Matthew C. Beard[*,‡]

[†]School of Optical and Electronic Information, Huazhong University of Science and Technology, Hubei 430074, China, [‡]Chemical and Material Sciences Center, National Renewable Energy Laboratory, Golden, Colorado 80401, United States, [§]Department of Physics, Colorado School of Mines, Golden, Colorado 80401, United States, [∥]Department of Chemistry and Biochemistry, University of Colorado, Boulder, Colorado 80309, United States, and [⊥]Center for Advanced Solar Photophysics, Los Alamos National Laboratory, Los Alamos, New Mexico 87545, United States

ABSTRACT We developed a strategy for producing quasi-spherical nanocrystals of anisotropic heterostructures of Cd/Pb chalcogenides. The nanostructures are fabricated *via* a controlled cation exchange reaction where the Cd^{2+} cation is exchanged for the Pb^{2+} cation. The cation exchange reaction is thermally activated and can be controlled by adjusting the reaction temperature or time. We characterized the particles using TEM, XPS, PL, and absorption spectroscopy. With complete exchange, high quality Pb-chalcogenide quantum dots are produced. In addition to Cd^{2+}, we also find suitable conditions for the exchange of Zn^{2+} cations for Pb^{2+} cations. The cation exchange is anisotropic starting at one edge of the nanocrystals and proceeds along the ⟨111⟩ direction producing a sharp interface at a (111) crystallographic plane. Instead of spherical core/shell structures, we produced and studied quasi-spherical CdS/PbS and CdSe/PbSe Janus-type heterostructures. Nontrivial PL behavior was observed from the CdS(e)/PbS(e) heterostructures as the Pb:Cd ratio is increased.

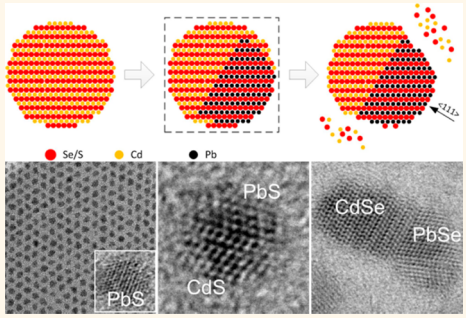

KEYWORDS: quantum dots · heterostructures · cation-exchange reactions · synthesis · lead chalcogenide

Complex and novel colloidal nanocrystals may be prepared by cation exchange reactions.[1−4] Generally, cation exchange reactions in colloidal nanocrystals have been shown to preserve the size and morphology of the reactant nanocrystals, producing heterostructures[5,6] and crystals whose phase[7] and shape[8] are often not accessible by conventional hot-injection[9] or heat-up[10] syntheses. The cation exchange reaction involves formation of a new solid phase and ligation of the exchanged cation in solution. Therefore, the thermodynamic driving force for the exchange is a balance between the solvation energy of the cation and the lattice binding energy before and after exchange.[2,11] The exchange of Pb^{2+} for Cd^{2+} in presynthesized PbE (E = S, Se, or Te) nanocrystals is commonly used to prepare heterostructured nanocrystals[6,12−14] made of Pb and Cd chalcogenide compounds. We recently discovered an effective reverse exchange that is the direct replacement of Cd^{2+} for Pb^{2+} in presynthesized CdE nanocrystals allowing for greater flexibility in the design of novel nanoheterostructures.[15] The reverse cation exchange reaction was achieved by modifying the ligating environment, which in turn alters the redox potentials of the cations in solution.[16] Our cation exchange reaction is promoted by using $PbCl_2$ in oleylamine (OLA). In our previous reports, we found evidence that Cd and Cl reside at the surface of the resultant PbSe QDs.[15] In our laboratory, we find that solar cells fabricated using these QDs produced *via* cation exchange exhibit both a higher power conversion efficiency (6.2% for PbSe[15] and 7.2% for PbS[17]) and better air stability when compared to solar cells fabricated from PbSe or PbS QDs that were synthesized from the standard PbO protocol.[18] For PbSe QDs, we showed that the enhanced stability can mainly be attributed to the Cl surface passivation and residual Cd does not play a large role.[15]

Herein, we further explore this new chemistry and show that it is general for the CdE to

* Address correspondence to matt.beard@nrel.gov.

Received for review March 27, 2015 and accepted July 10, 2015.

Published online July 10, 2015
10.1021/acsnano.5b01859

PbE QD exchange. We also demonstrate that PbS QDs can be prepared from ZnS QDs implying that cation exchange reactions can be further generalized. Finally, we develop nanocrystal heterojunctions that are anisotropic in composition yet quasi-spherical in shape, called Janus particles, where one-half of the nanocrystal is composed of PbE and the other half of CdE.

Heterostructured nanocrystals are a class of promising systems in which the different components of the structure can be independently tuned, giving rise to new optical and electronic properties not accessible in bulk systems. Tuning of the band alignment between the two halves of the heterostructure provides a new capability for controlling the relaxation pathways of photogenerated carriers because of the ability to perform "wavefunction engineering", *e.g.* tuning the band offsets and controlling the electron−hole (e-h) wave function overlap. Novel nanoheterostructures such as core/shell,[6] core/shell/shell,[19] dot-in-rod, dot-on-rod,[20] and heterotetrapods[19] have all been developed over the past few years with the intent to control energy and charge relaxation pathways. Recently, core/shell QDs with thick shells, or giant-QDs (g-QDs), where the shell is CdS and the core is CdSe, have been explored because they exhibit some fascinating properties, such as decreased single particle photoluminescence blinking,[21] emissive biexciton states,[22] and controllable separation between the emitting and absorbing states (variable Stokes-shift).[23,24] Extension of these concepts to infrared QDs by employing the PbE/CdE system has been explored by a number of researchers. Lee *et al.* showed that in core/shell/shell structures with a PbSe core, the photoluminescence (PL) lifetime could be increased by 2 orders of magnitude.[19] Giant QDs of PbE/CdE,[25] where the PbE component is the core, have been developed in analogy to the CdSe/CdS g-QDs system. Lin *et al.* demonstrated dual emission from PbSe/CdSe system. They find that the electron delocalizes across the structure (so-called quasi-type II band offset) leading to a reduced e-h wave function overlap while the hole undergoes a slow relaxation from a localized state in the shell to the core allowing for emission from both shell and core states.[25] Cirloganu *et al.* took advantage of this slowed hole relaxation to demonstrate that in thick shell PbSe/CdSe core/shell nanocrystals the multiple exciton generation/carrier multiplication (MEG/CM) efficiency could be improved considerably over that of a single component nanocrystal.[26]

Such structures, with improved MEG, would be very useful for solar cell applications,[27] but they suffer from the inability to extract the hole. The electron is delocalized across core and the shell, while the hole localized within the PbE core of the nanostructure. Ideally, an inverted core/shell structure, where PbE is the shell, would provide both high MEG as well as access to both carriers: the hole would be localized to the shell while the electron would be delocalized across the entire nanostructure. Elongated anisotropic systems, such as nanorods (NRs), also could allow access to both carriers, at different spatial positons and there have been several methodologies developed to produce such structures. Kudera *et al.* demonstrated that CdS NRs can be used as seeds to grow PbSe QDs on the ends of the rods.[28] Luther *et al.* developed a two-step cation exchange reaction to produce PbS NRs from CdS NRs with Cu_2S as an intermediate between the CdS and PbS system.[29] They found that the reaction could be controlled to produce rods where half is CdS and half is PbS. Nanayakkara *et al.* employed scanning Kelvin probe microscopy to study the band offsets in the CdE/PbE NRs and found large built-in fields that occur at the interface.[20] However, forming close-packed arrays necessary for QD photovoltaic systems may be difficult with such elongated nanostructures. Recently, Ha *et al.* constructed large, 20 nm, spherical heterostructured particles of ZnS/CuS by a controlled cation exchange of Cu^{2+} for Zn^{2+}.[30] In their reaction, the cation exchange starts at opposite edges of the nanocrystals producing spherical heterostructures that "sandwich" the CuS between ZnS (dual interfaces). The heterostructures presented here are smaller and quantum confined heterostructures with a quasi-spherical shape yet anisotropic composition, which could allow for access to electrons and holes within an amenable packing geometry.

EXPERIMENTAL SECTION

The reactions described here start by heating $PbCl_2$ in oleylamine (OLA) at 140 °C for 30 min and then cooling to room temperature; the resulting complex forms a viscous solution or gel. The $PbCl_2$/OLA gel is then reheated to a temperature that ranges from 80 to 190 °C depending on the starting and desired ending QD size (details are provided in the Methods section and the Supporting Information). The presynthesized CdE QDs[31] (in toluene or octadecene) are then rapidly injected followed by controlling the bath temperature according to the desired product. The color of the solution changes immediately upon the injection of CdE QDs, indicating that the cation exchange reaction proceeds very quickly.[1] Oleic acid (OA) is added to the reaction mixture to remove unreacted $PbCl_2$ and replace OLA ligands that are weakly bound to the QD surfaces. The resulting QDs can be isolated using polar solvents and centrifugation and redispersed into nonpolar solvents similar to washing procedures used for traditional PbE QD syntheses.

RESULTS

Synthesis of PbS QDs *via* Conversion of CdS QDs. Phase pure PbS QDs can be synthesized directly *via* the complete cation exchange described above when the starting CdS QDs have sizes that range from about 1.7 to 6 nm.

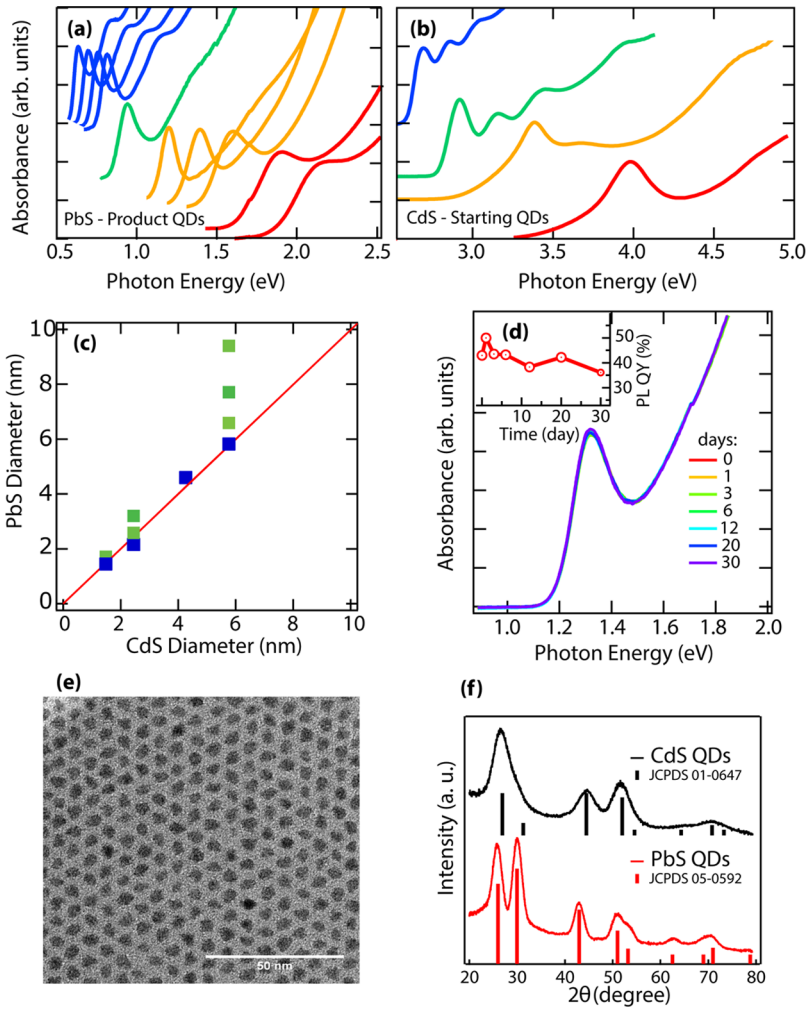

Figure 1. (a) Absorption spectra of resulting PbS QDs synthesized from starting CdS QDs shown in (b). The color of the PbS traces indicates from which CdS QD batch the resulting PbS QDs were synthesized. The spectra are vertically offset for clarity. In (c), we plot the resulting PbS QD diameter as a function of the starting CdS QD diameter. The blue squares are for syntheses where the reaction was stopped immediately after the injection of CdS QDs, while the green squares show the size for PbS QD samples that were allowed to continue growing. (d) Absorption spectrum and PL QY (inset) of ~3 nm PbS QDs dispersed in hexane and stored in air for 30 days. (e) A typical TEM image of the PbS QDs synthesized from CdS QDs and (f) the corresponding XRD patterns of the starting CdS QDs and ending PbS QDs demonstrating the complete exchange from CdS to PbS.

The small limit of achievable sizes is only constrained by the synthetic protocol for making the smallest starting CdS QDs. Since the size of the resulting PbS QDs is influenced by the starting size of the CdS QDs, we can produce very small PbS QDs with a diameter of 1.7 nm. This corresponds to a first exciton peak at 570 nm (2.17 eV), which to our knowledge is close to the smallest PbS QDs produced. In Figure 1a, we show the spectra of the resulting PbS QDs that were obtained from the starting CdS QDs whose spectra is displayed in Figure 1b. The colors of the PbS traces correspond to those of the starting CdS QD spectra. In Figure 1c, we show the sizes of the fully exchanged PbS QDs (blue squares) plotted against the corresponding starting CdS QD sizes. The diameters are determined from standard sizing curves that relate the first exciton absorbance to the QD diameter for both CdS[32] and PbS.[33] The full exchange of smaller CdS QDs (1.48 nm $\leq d \leq$ 5.72 nm) was achieved by increasing the solution temperature at injection, and in some cases accompanied by small increases in reaction time (a summary of the synthesis conditions for each of the points in Figure 1c are shown in Supporting Information Table S1). Within the synthesis parameter space explored here, larger CdS QDs (>6 nm) could not be exchanged for two reasons. As evidence by the summary of synthesis in Supporting Information Table S2, the exchange of increasingly larger CdS QDs required significant increases in temperature (*e.g.*, from 80 °C for 2.43 nm CdS to 190 °C for 4.26 nm CdS). The usable temperature range is limited to approximately ≤200 °C because the $PbCl_2$/OLA mixture becomes unstable and a precipitate is formed above 200 °C. Increasing the reaction time, on the other hand, led to significant issues of nanoparticle coagulation. However, the range of obtainable fully exchanged PbS

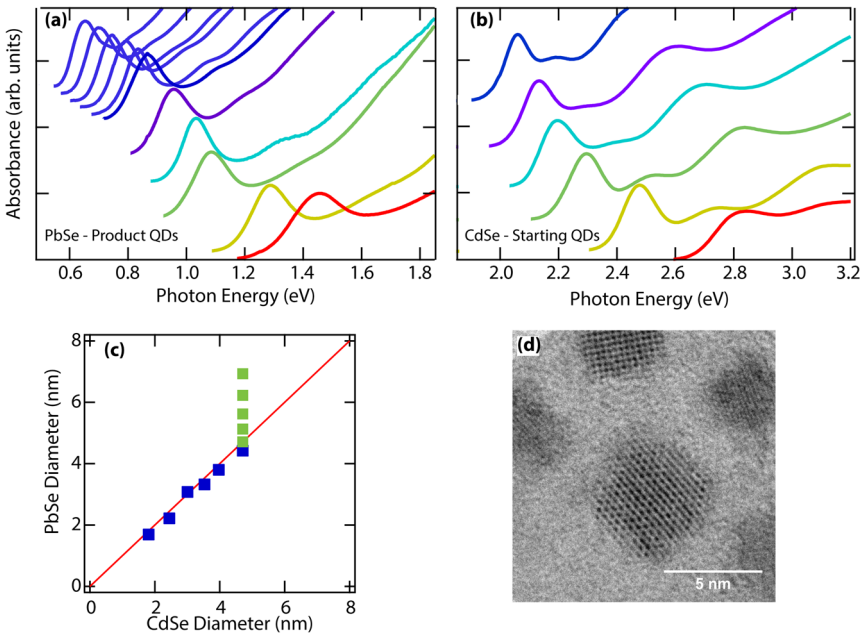

Figure 2. (a) PbSe QDs that result from the cation exchange reaction of the starting CdSe QDs shown in (b). (c) The resulting size of the PbSe QDs corresponds to the size of the starting CdSe QDs. (d) HRTEM shows that the majority of the exchanged QDs are highly crystalline.

QD sizes could be expanded by growing PbS QDs to sizes larger than that of the starting CdS QDs. This was done by increasing the reaction time, beyond that necessary to obtain PbS QDs of the same size as the starting CdS QDs. The QDs continue to grow *via* dissolution of smaller QDs and growth of larger QDs similar to what has been observed for the preparation of PbS QDs from $PbCl_2$/OLA.[34] Thus, the cation exchange reaction likely is accompanied by a small amount of dissolution at the edges of the nanocrystals that is more pronounced for the smaller QDs within the ensemble.

We characterized the PbS QDs using TEM, XPS, PL, XRD, and absorption spectroscopy. XPS data (Supporting Information Figure S2) shows that the residual amounts of Cd and Cl compared to Pb are 3.5% and 39%, respectively, for ~3 nm PbS QDs, and vary with size consistent with reports where Cd and Cl passivate QD surfaces.[33,35−37] The presence of Cd and Cl on the QD surfaces is further supported by their removal as a result of various ligand treatments when preparing QD films.[17] The resulting PbS QDs exhibit enhanced air stability when dispersed in hexane, as shown in Figure 1d. The first exciton peak does not shift during the storage time of 30 days and the photoluminescence quantum yield (PL QY) remains at values greater than ~40% during this time. The TEM image in Figure 1e shows the monodispersity of the as-synthesized PbS QDs and XRD patterns (Figure 1f), demonstrating the transformation from zinc blende (CdS) to rock salt (PbS).

Synthesis of PbSe QDs *via* Conversion of CdSe QDs. In a similar fashion to the exchange of CdS QDs for PbS QDs, CdSe QDs ranging in size from ~2 to ~5 nm can undergo complete cation exchange for PbSe QDs. Larger PbSe QDs (up to ~7 nm) can be prepared by continuing the growth after the initial cation exchange with the introduction of additional Se precursor (TOPSe). Figure 2 displays the spectra of the PbSe QD (a) products with the CdSe (b) starting QDs. As in the case of the CdS exchange to PbS, the final size of the PbSe QDs is influenced by the size of the starting CdSe QDs. For complete cation exchange, the PbSe QD size is only limited on the small side by the starting CdSe QDs. Further details of the synthesis and as well characterization, including XRD, are provided in our earlier publication.[15]

Synthesis of PbTe QDs *via* Conversion of CdTe QDs. We also demonstrate that PbTe QDs can be prepared from presynthesized CdTe QDs. We prepared CdTe QDs with diameters of 3 and 3.6 nm (Figure 3b) and injected these into the $PbCl_2$/OLA mixture at 180 °C. The resulting PbTe absorbance is shown in Figure 3a, and the resulting PbTe QD average diameter was determined to be 2.4 and 4.3 nm from standard size *vs* first exciton absorption curves.[32,38] The XRD (Figure 3c,d) analysis confirms the conversion of CdTe to PbTe. We find for the CdTe/PbTe system, both the size of the resulting QDs and size distribution are worse than those obtained for the PbS and PbSe QDs presented above. However, PbTe QDs produced *via* the standard PbO synthesis are very unstable and degrade in air in only a few hours.[39] The cation exchanged PbTe QDs produced here are stable over the course of at least a few weeks when stored in air, thus providing impetus to further develop this synthetic protocol which will be the subject of future publications.

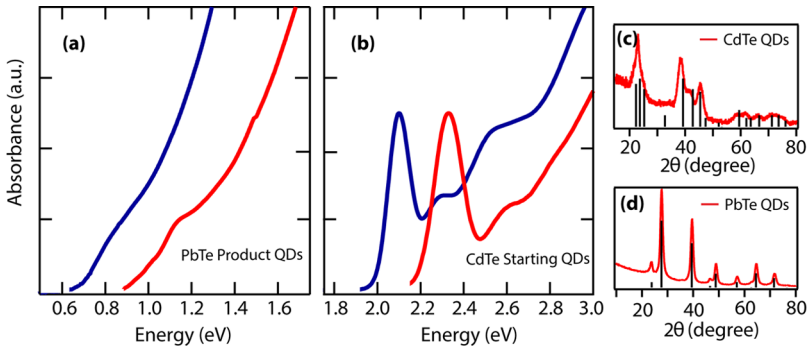

Figure 3. Absorption spectra of the final PbTe QDs (a) that are synthesize from CdTe QDs (b). The XRD patterns demonstrate the conversion of CdTe (c) to PbTe (d). JCPDS cards 01-075-2083 and 01-072-6645 were used for the standard patterns of CdTe and PbTe, respectively.

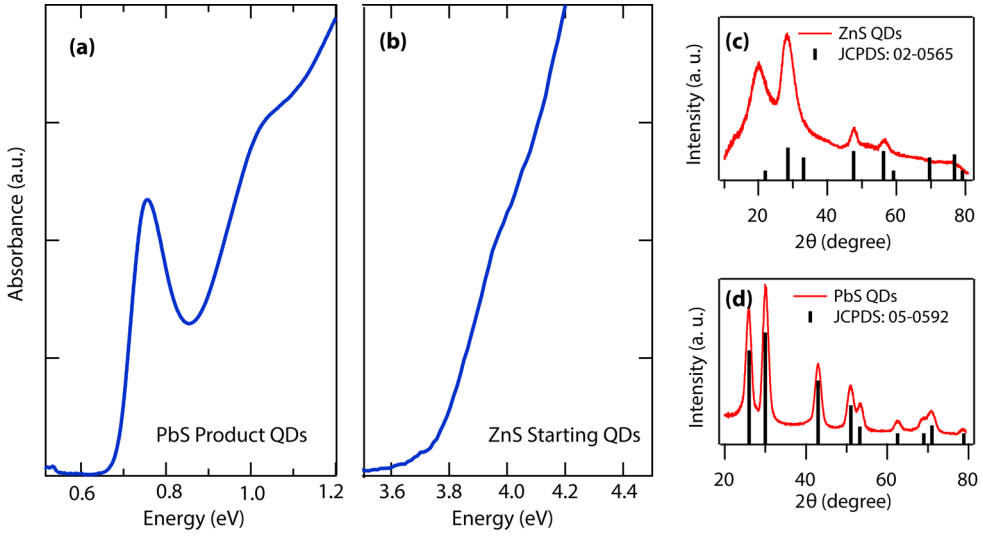

Figure 4. Absorption spectra of the resulting PbS QDs (a) and starting CdS QDs (b). XRD patterns of the starting ZnS (c) and final PbS QDs (d) demonstrating the complete conversion from ZnS to PbS.

Synthesis of PbS QDs *via* Conversion of ZnS QDs. To test the versatility of this cation exchange, we investigated exchange of a variety of metal sulfide nanoparticles, including Ag_2S, Cu_2S, ZnS, SnS, MnS, and HgS, which were injected into the hot $PbCl_2$/OLA complex. Among those listed metal sulfide nanoparticles, only ZnS works for the cation exchange *via* the synthetic protocol discussed here. Figure 4 shows the absorption spectra of the starting ZnS QDs (b) and the resulting PbS QDs (a). Figure 4c,d confirms the transformation of the crystalline structure.

Synthesis of PbE *via* Conversion of CdE Nanorods. We also attempted to use CdE NRs to directly produce PbE NRs. However, both the CdSe and CdS NRs transformed to QDs with a broad size dispersion, as shown in Supporting Information Figure S4. Figure 5 shows the evolution of the absorption spectrum and shape of the nanocrystals when CdSe NRs are used for the cation exchange at 80 °C. At this temperature, the CdSe NRs are transformed to PbSe QDs slowly, and we can stop the reaction at various stages to study the evolution of the cation exchange. As shown in Figure 5b−d, the transformation of CdSe NRs to spheroid PbSe nanocrystals is not immediate but occurs between 1 and 15 min of reaction. A similar transformation of CdSe NRs to spheroid particles, of Ag_2Se, was reported by Son *et al.*[1] The authors observed that the shape asymmetry was retained only for starting NRs that were thinner than a particular size (4 nm, in their system). They suggested that this cutoff-width for shape transformation corresponds to a reaction zone width, which is the length of the reaction front within which the phase and morphological transformations occur. A similar situation may play a role here, and the characteristic reaction zone width may be smaller than the NR width (*e.g.*, half or quarter of the NR width) depending on the nucleation density of the PbSe phase along the NR. (For example, Ag_2S nucleates throughout the entire NR surface when exchanging CdS NRs.[5,40]) The small size of the resulting PbSe QDs (~5 nm) compared to the starting size of the CdSe NRs (~5.4 nm × 30 nm) indicates that the CdSe NRs split into multiple PbSe QDs. This suggests that the reaction zone width is equal to or even less than the starting CdSe NR width,

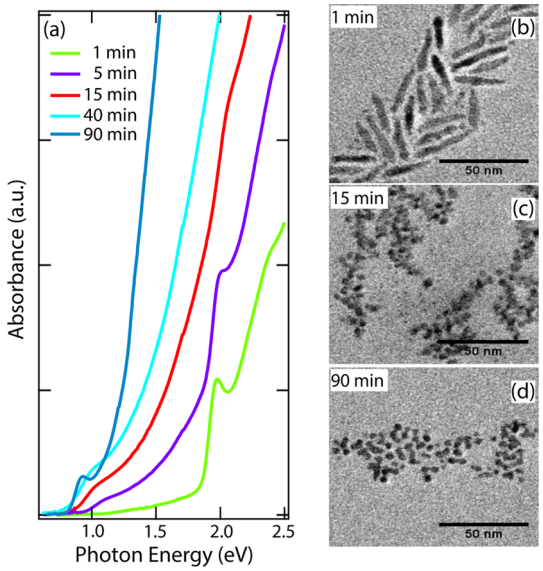

Figure 5. (a) Evolution of the absorption spectra of nanocrystals during cation exchange reaction using CdSe NRs as the starting particles and a bath temperature of 80 °C. (b–d) TEM images showing that the nanorod shape is not retained during the cation exchange and spherical PbSe QDs are produced after 90 min of reaction time.

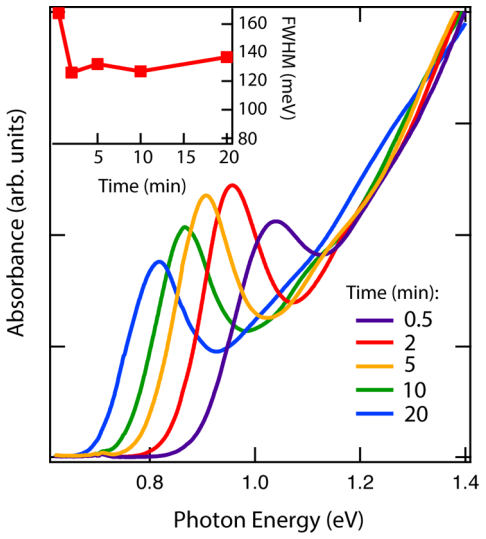

Figure 6. Evolution of absorption spectrum of PbSe QDs when CdSe (with an exciton peak at 580 nm) QDs were injected into $PbCl_2$/OLA at 150 °C. The inset shows the evolution of the fwhm of the 1st exciton peak as a function of reaction time, indicating that size focusing occurs within the first 2 min after injection of the precursor CdSe QDs.

despite the full shape transformation, because a reaction zone width closer in scale to the NR length (tens of nm) is more likely to result in larger PbSe nanocrystals—with the limit being a full transformation of one NR to one nanocrystal—which would be thermodynamically preferred due to a reduced surface area compared to the small PbSe QDs observed here.

Reaction Mechanism. To further study the reaction, we performed two experiments. First, we produced PbSe QDs from CdSe QDs, but rather than quenching the reaction immediately upon injection of CdSe, we maintained the temperature and monitored the absorption spectra (Figure 6). The cation exchange begins immediately upon injection of the CdSe QDs and then continues until complete. When the temperature is maintained, continued growth of PbSe QDs occurs even after complete cation exchange has occurred. Size focusing occurs within the first 2 min (see inset of Figure 6). Our previous work demonstrated that growth of PbS/PbSe QDs, in the $PbCl_2$/OA heterogeneous system, occurs through dissolution of smaller nanoparticles and growth of larger nanoparticles.[34] According to classical theory, size focusing only happens at a high oversaturation condition.[41] As no Se precursor is added here, the oversaturation condition can either be attributed to dissolution of CdSe during the cation exchange, which can then act as the selenium source for further growth of the PbSe QDs, or dissolution of smaller PbSe QDs once formed. In preparation of the larger PbSe particles (>5 nm), additional Se precursor can be added during the later stages of particle growth so that oversaturation conditions can be maintained (Figure 2, green squares).

In the second experiment, we monitored the exchange of CdS to PbS at lower temperatures, where intermediates can be captured. Therefore, we can study how the cation exchange proceeds *via* the propagation of the phase boundary across the crystallite.[2] Similar to the isovalent exchange of Pb^{2+} to Cd^{2+},[2] the reverse exchange of Cd^{2+} to Pb^{2+}, described here, is thermally activated and allows the capture of intermediate states during the synthesis. Figure 7a shows the evolution of absorption spectra of the nanoparticles during the synthesis of PbS QDs when large CdS QDs (~5.7 nm) are used as the starting point. At the earliest times (10 s), the calculated PbS domain size is smaller than the 5.7 nm starting QD size (Figure 7c) and only reaches the starting size after ~90 s. (The PbS domain size is calculated using the Moreels *et al.*, first exciton peak center *versus* QD size chart.[33]) At the same time, the concentration of PbS particles (calculated based on Beer's law[33,34]) remains constant in the first 40 s and then decreases thereafter (Figure 7b). Therefore, the invariable particle concentration and the smaller starting size of the PbS component compared to the starting CdS QDs suggest that partial exchange is occurring during the first ~50–90 s. The increase of the PbS size during the partial exchange suggests propagation of the phase boundary. In addition, during the partial exchange, the fwhm of the first exciton PbS peak remains narrow. Because the solution is vigorously stirred, the temperature fluctuation across the sample solution is very small, resulting in narrow size dispersion of the converted PbS area. When the whole CdS QD is completely converted to PbS (at about 40 s for these conditions), the nanoparticles grow *via* dissolution of smaller PbS QDs,[34] confirmed by the

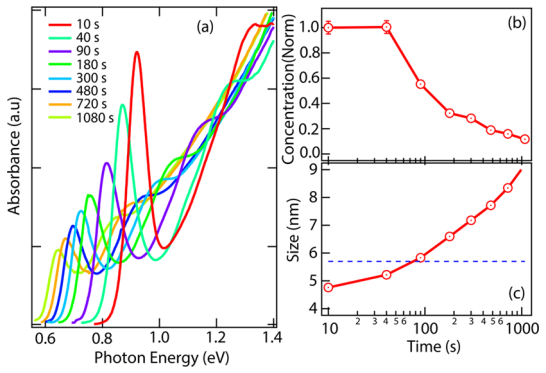

Figure 7. Evolution of the absorption spectra (a), particle concentration (b), and size (c) of PbS nanocrystals after 5.7 nm CdS QDs were injected into $PbCl_2$/OLA at 190 °C and the reaction temperature was maintained at 180 °C. The dotted line in (c) represents the size of the starting CdS QDs.

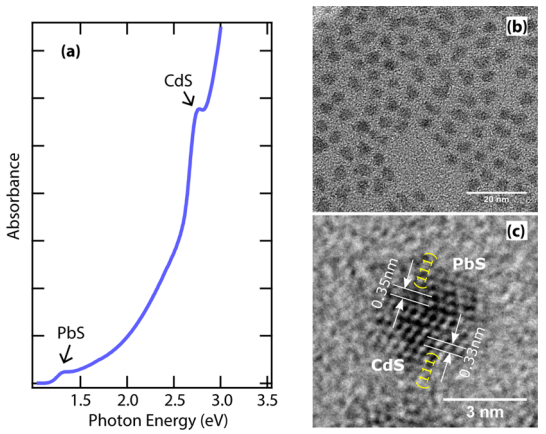

Figure 8. Heterostructured spherical nanocrystal where approximately half of each QD is PbS and half is CdS. The absorption spectrum (a) shows features that can be assigned to the CdS and PbS and the TEM images (b and c) of partially exchanged CdS QDs demonstrate both the spherical nature as well as that each QD consists of a heterostructure comprising CdS and PbS.

decrease of the PbS concentration and increase of the fwhm between 90 and 1080 s.

Preparation of CdE/PbE Heterostructures. One of the advantages of cation exchange reactions is that anisotropic morphologies can be readily accessed that are otherwise difficult to prepare.[29,30] Figure 8 shows the absorption spectrum (a) and TEM images (b and c) of partially exchanged CdS QDs. The boundary between different domains can be distinguished in HRTEM images (Figure 8c). The absorption spectrum in Figure 8a shows the first exciton peaks of both the CdS and PbS QDs. As the cation exchange is thermally activated, the size of converted PbS depends directly on the initial temperature in the partial exchange. Three samples were prepared with varying amounts of PbS exchange, with the results depicted in Figure 9. For each reaction, the starting CdS QDs (5.7 nm diameter) are the same and changing the reaction temperature controls the relative amounts of CdS and PbS components in the CdS/PbS heterostructure. For the reactions conducted at higher temperatures, the first exciton peak of the PbS component redshifts, while that of CdS disappears gradually (Figure 9a), indicating the increase of PbS at the expense of CdS. The increase of the (200) and (400) diffraction intensity of PbS at higher reaction temperature (Figure 9b) also confirms the extension of PbS segments at higher reaction temperatures. For the reaction conditions corresponding to the lowest temperature of 110 °C, we find two emission peaks at ~870 and 1040 nm (Figure 9c). Interestingly, both the band edge emission of CdS and the native CdS surface trap emission[42,43] (see Supporting Information Figure S5) become negligible after the nucleation and growth of PbS. We assign the 1040 nm emission to the direct band edge emission in PbS. The higher energy transition (870 nm) is not high enough to arise from the direct CdS band emission since this occurs at wavelengths smaller than ~500 nm for these samples. The 870 nm emission also is too low in energy and too narrow to arise from the commonly observed native CdS trap emission (Supporting Information Figure S5).[42,43] Possible sources for this 870 nm emission are cross-emission from the conduction band of CdS to the valence band of PbS and trap emission specific to defects at the PbS/CdS interface.

As the PbS domain increases (Figures 9 d,e), the PbS band-edge emission redshifts in accordance with decreasing quantum confinement. Concurrently, the emission spectrum becomes dominated by the PbS band-edge emission while other emissions, such as from PbS/CdS interface traps or cross-emission observed in Figure 9c, become negligible. Interestingly, the native CdS trap-emission, clearly visible in the starting samples (Supporting Information Figure S5), is quenched upon nucleation and growth of PbS domains. Therefore, the addition of just a small amount of PbS, and/or MCl_2 (where M is Cd or Pb), may passivate some traps in CdS or create competing relaxation pathways for the photogenerated carriers that bypass the trap state in CdS. We also find similar effects when the size of the starting CdS is changed (Supporting Information Figure S6): the PL spectra of CdS/PbS heterostructures with different CdS:PbS ratios is consistent with the results shown in Figure 9.

A two-step synthetic protocol was used for the synthesis of Janus-like heterostructures of CdSe/PbSe. (Under similar, one-step exchange, synthetic conditions described above for the preparation of CdS/PbS heterostructures, preparation of CdSe/PbSe heterostructures results in larger coagulated particles that are not stable in solution; this is further discussed in the Discussion section below.) First, a minimal amount of cation was exchanged from CdSe to PbSe at a relatively low temperature (here 60 °C) yielding QDs with the absorption spectrum shown in Figure 10a (red trace). Then, the slightly exchanged CdSe QDs were used as

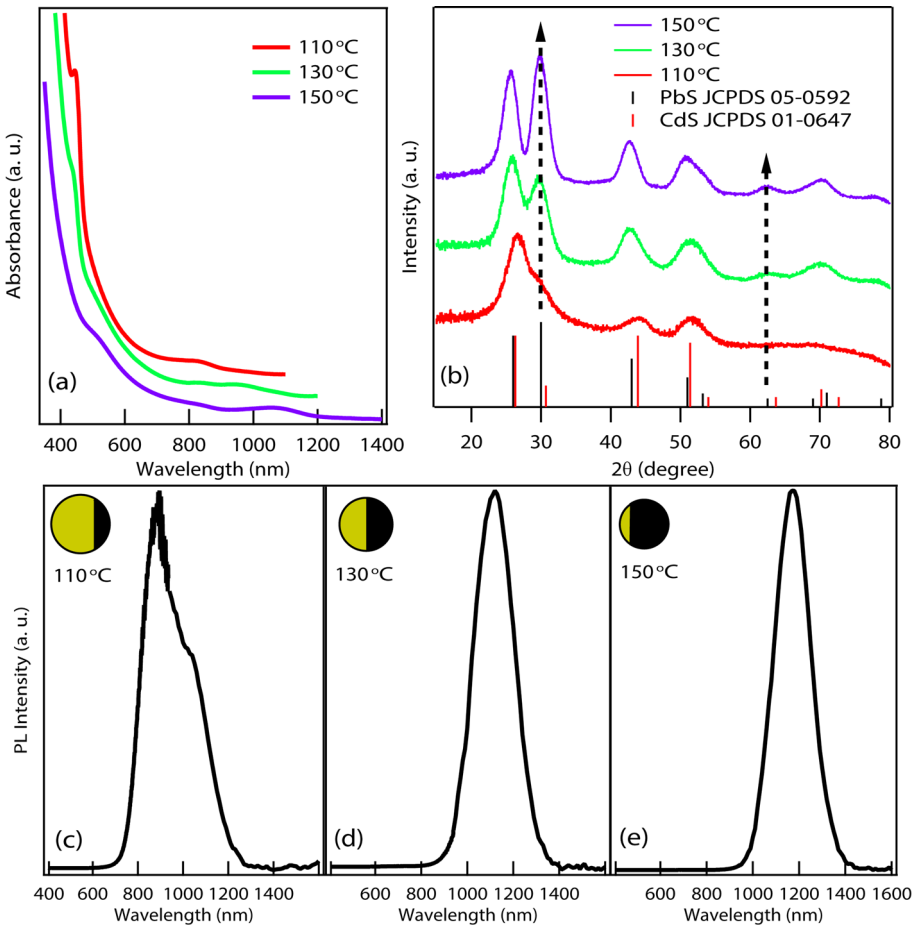

Figure 9. Absorption spectra (a), XRD patterns (b), and PL spectra (c–e) of the CdS/PbS heterostructures synthesized at different temperatures. The ratio of PbS:CdS increases with higher temperatures, which is schematically shown by the spheres in panels c–e (yellow represents CdS and black represents PbS).

seeds to further grow PbSe domains on the CdSe QDs in 1-octadecene using Pb-oleate and trioctylphosphine selenide (TOPSe) as the Pb and Se precursors, respectively (details in the Methods section). Figure 10a (blue trace) shows the absorption of the two-step synthesized CdSe/PbSe heterostructure whose absorption redshifts substantially compared to that of the slightly exchanged CdSe QDs, confirming the growth of the PbSe domain. There are two possible reaction pathways that could result in the heterostructures; (1) the PbSe can grow epitaxially onto the slightly exchanged CdSe QDs or (2) the PbSe domain increases *via* further cation exchange. A control experiment was performed to determine whether the growth of PbSe originates from further cation exchange or adsorption of Pb and Se monomers. The slightly exchanged CdSe seeds were subjected to identical conditions but without the injection of TOPSe. Compared to the starting material, the product of the control experiment changed very little (Figure 10a green dash trace). Therefore, we conclude that the growth of the PbSe mainly arises from the epitaxial growth upon the exchanged part (PbSe) of the slightly exchanged CdSe/PbSe structures. TEM images show that the nanoparticles retained their individuality after the growth of PbSe (Supporting Information Figure S7). The sharp interface between the two domains can be readily observed (Figure 10d). Note that the nanoparticles are randomly oriented on the TEM grid and not all of the particles are oriented such that they show the interface. In some particles, the PbSe component is observed at two opposite sides of CdSe (Figure 10e), suggesting that cation exchange proceeds along specific crystallographic planes of the CdSe QDs.

The variation of PL emission of the CdSe/PbSe heterostructures while changing the CdSe:PbSe ratio is consistent with that of CdS/PbS heterostructures. The CdSe band edge emission and the native CdSe trap emission both become negligible after addition of PbSe. With small domain sizes of PbSe, a higher energy peak at ~900 nm is visible in addition to the PbSe band edge emission at 950 nm. As in the case of PbS/CdS discussed above, the higher energy peak may arise due to, for example, cross-emission from the CdSe conduction band to the PbSe valence band or trap emission due to defects at the CdSe/PbSe interface. As the PbSe domain size increases, the band edge emission of PbSe redshifts (to 1330 nm for approximately equal

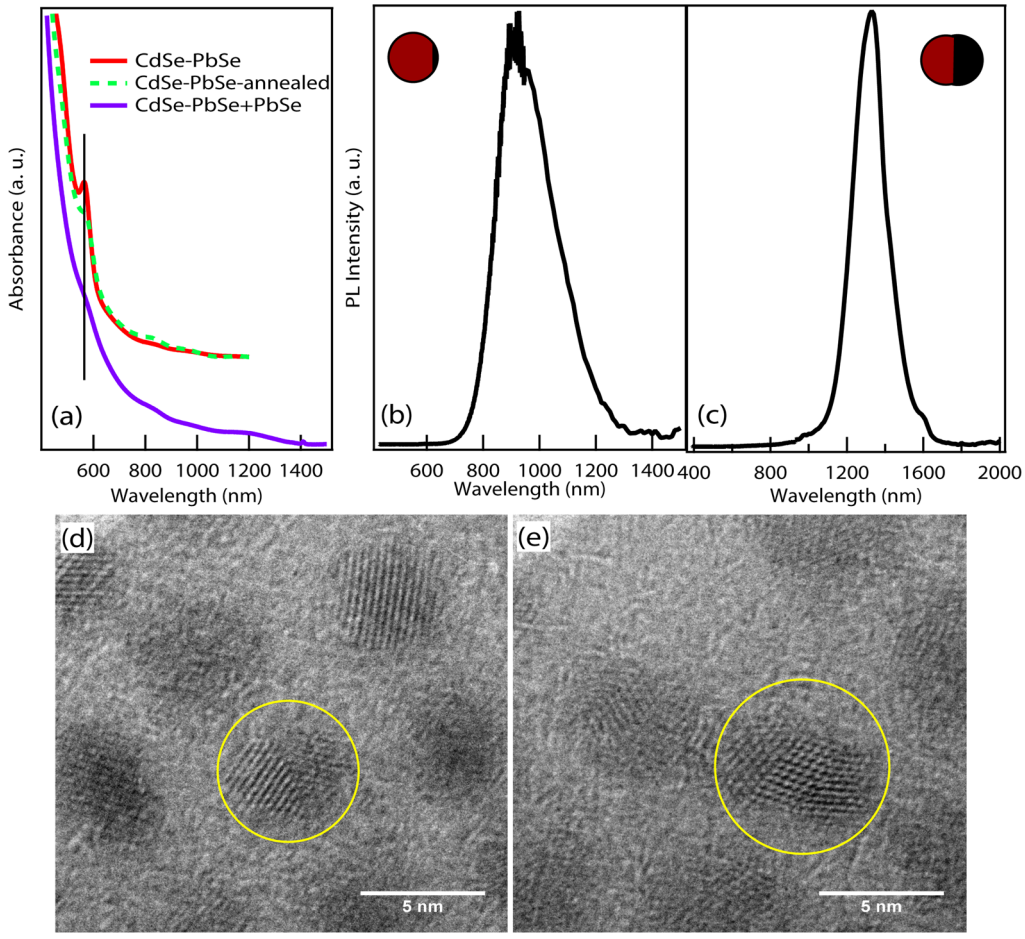

Figure 10. (a) Absorption spectra of slightly exchanged CdSe seeds (red line), products of two-step-synthesis with (blue line) and without (green dash line) the additional growth step using TOPSe. PL spectra of the slightly exchanged CdSe/PbSe seeds (b) and CdSe/PbSe heterostructures (c). The ratio of PbSe:CdSe increases in the second step of the synthesis, which is schematically shown by the spheres in (b) and (c), where red represents CdSe and black represents PbSe. TEM images (d and e) of the CdSe/PbSe heterostructures synthesized by the two-step method (with addition of TOPSe).

proportions of CdSe:PbSe) and the higher energy peak disappears.

DISCUSSION

One may discuss the cation exchange process in terms of a reaction zone width,[1,40,44] within which there are fluxes of species entering and of species leaving the reaction zone. In the syntheses shown here, the Pb^{2+} cation is the entering species and the Cd^{2+} cation is the exiting species, which is swept away at the surface. This is an unsteady state process, but at a fixed time near the beginning of the exchange, we expect the reaction zone width to be greater with elevated temperatures due to the increased diffusion rate of the cations. We find that a higher temperature or increased time is necessary to completely exchange CdSe QDs than CdS QDs of any particular size. This suggests that the reaction zone width is larger for the CdS/PbS system than for the CdSe/PbSe system. This is consistent with reports of faster Cd interdiffusion in CdS than in CdSe.[45]

Both the cations and anions may be mobile in the crystal.[1] Generally, the cation diffusion rate is much greater than that of the anion due to the size difference of the ions and the cations may be perceived as diffusing within a rigid anion lattice.[45,46] This is consistent with the observations of the QD size remaining constant after full conversion to PbE (*i.e.*, Figures 1c and 2c). However, at a high enough temperature such that the reaction zone width is much larger than the nanocrystal size, the nanocrystal may undergo a morphological transformation to a thermodynamically favorable shape.[30] However, when the reaction zone width is smaller than the QDs, the situation is more complex.[30] For isotropic cation exchange, the reaction zone can be inside the nanocrystal, in which case the cation exchange proceeds *via* isotropic propagation of the reaction front, thus the starting shape is retained.[1] For anisotropic cation exchange, the reaction zone may be exposed on the surface (*i.e.*, along a preferential crystal plane). Indeed, the exchange of CdE for PbE proceeds anisotropically, as indicated by the TEM images in Figures 8c, 10d,e, and 11a,b. Anisotropic cation exchange may also result in reduced ligand coverage along a particular plane during the reaction allowing

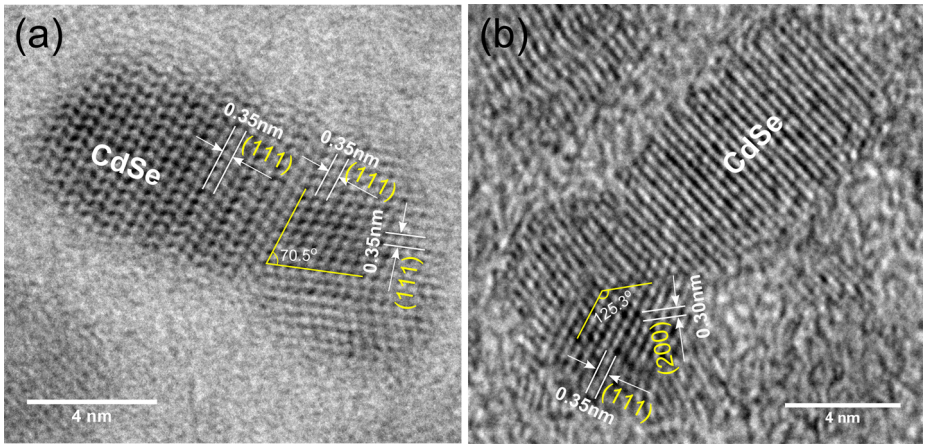

Figure 11. TEM image of partially exchanged CdSe QDs (two or three nanoparticles are fused together). (a) The PbSe and CdSe domains form two (111) interfaces showing an angle of 70.5°, which equals the angle between two (111) planes in a cubic crystal. (b) PbSe domain terminated with (111) and (200) planes at the interface of PbSe and CdSe.

adjacent nanocrystals to coagulate *via* fusion at the exposed area. Coagulation is observed with exchange of CdSe for PbSe and CdTe for PbTe (Supporting Information Figure S8), and least of all with exchange of CdS for PbS (Figure 8b). Increased coagulation and size distribution may be explained by the relative rigidity of the anion sublattice, which follows the order of MS > MSe > MTe (M = metal) per their lattice formation energies and hardness. For example, the relative rigidity of the anion sublattice is lower for the Te case leading to poor preservation of the Te sublattice of the starting CdTe QDs and a greater degree of Ostwald ripening and/or fusion of nearby QDs.

The partial CdS(e) to PbS(e) exchanges do not produce core/shell structures. Instead, the cation exchange reaction starts at specific sites or planes (*i.e.*, (111)). In contrast to the reaction presented here, in the exchange of PbE to CdE, the reaction occurs isotropically and core/shell structures are prepared.[6,12,13,47] However, the reaction does proceed preferentially in the ⟨111⟩ direction with the formation of sharp $(111)_{PbSe}/(111)_{CdSe}$ interfaces.[12] Here, the partial exchange reaction also shows sharp (111) boundaries between the two phases (Figure 5c). The sharp anisotropic boundary and preferential crystallographic plane suggest that the cation exchange of CdS(e) to PbS(e) proceeds in a layer-by-layer fashion in the ⟨111⟩ direction. The fact that for both the Pb^{2+} to Cd^{2+} and the Cd^{2+} to Pb^{2+} reactions the (111) crystal plane plays a dominate role can be attributed to the arrangement of these planes. Specifically, the (111) planes consist entirely of either cations or anions in an alternating fashion. Theoretical calculations of partially exchanged CdSe/PbSe QDs suggest that there is an interfacial Se atomic layer that is sandwiched by a Pb layer on one side and a Cd layer at the other side in the ⟨111⟩ direction.[48] Such a configuration should produce a strain-free interface.[48] The partial exchange based on CdSe QDs confirms the formation of a sharp (111) interface despite the coagulation of the nanoparticles, as shown in Figure 11 and Supporting Information Figure S3. PbSe domains terminated with (100) planes are also observed at the CdSe/PbSe interface (Figure 11b), similar to recent theoretical and experimental studies,[49] though not as prevalently as interfacial (111) planes.

CONCLUSION

We develop cation exchange procedures to convert CdE or ZnE QDs to PbE where E = S, Se, or Te. The synthesized PbE QDs cover a large range of sizes. With XPS analysis, we find that residual Cd and Cl remain following the cation exchange. Considering our earlier studies, where that residual Cd and Cl are removed through ligand treatments, we suggest that the residual Cd and Cl reside near the QD surfaces.[15,17] The residual Cd and Cl contribute to long-term air-stability of the QDs that are dispersed in hexane and stored in air. The exchange of Cd^{2+} to Pb^{2+} is anisotropic, proceeding preferentially along the ⟨111⟩ direction with the formation of a sharp (111) epitaxial interface. For the cation exchange reaction to proceed completely, the size of the starting QDs needs to be less than 6 nm for CdS and 5 nm for CdSe, but larger QDs can be grown by prolonged growth and, in the case of PbSe QDs, by introducing additional chalcogenide precursor. The cation exchange protocol does not preserve the shape of the nanocrystals when nanorods of CdSe or CdS are used.

The thermally activated Cd^{2+} to Pb^{2+} exchange, controlled by reaction temperature and time, proceeds *via* the propagation of the reaction front. Using this controllable cation exchange, we produced heterostructures containing CdS(e) and PbS(e), which exhibit interesting optoelectronic properties that could be tailored for potential applications in a variety of fields. The controllable cation exchange demonstrated here shows another synthetic strategy for high quality QDs, in addition to other hot-injection and heating-up

methods, which could be applicable to other material systems.

This approach for making QDs has already shown promise for QD solar cells. We recently demonstrated that the QDs synthesized *via* cation exchange and the solar cells made from them exhibit improved air stability and higher power conversion efficiencies (6.2% for PbSe[15] and 7.2% for PbS[17]) when compared to solar cells containing QDs fabricated from the standard approach utilizing PbO. The heterostructures prepared by the approach described here could furthermore prove very useful for enhancement of solar cell efficiencies through harnessing MEG.[27]

METHODS

Materials. $PbCl_2$ (99.999%), oleylamine (OLA, tech. grade, 70%), CdO (≥99.99%), oleic acid (OA, tech. grade, 90%), 1-octadecene (ODE, tech. grade, 90%), selenium powder (99.99%), trioctylphosphine (TOP, tech. grade, 90%), sulfur powder (99.98%), ammonium sulfide (40−48 wt % in H_2O), chloroform (anhydrous, 99+%), tetrachloroethylene (TCE, ≥99.9%), hexane (95%), and ethanol (≥99.5%) were purchased from Sigma-Aldrich. Lead oxide (PbO, 99.99%) was purchased from Alfa Aesar. All the chemicals were used as received.

Synthesis of CdS QDs. Small CdS QDs were synthesized following the method developed by Robinson *et al.*[50] but without drying the sulfur precursor, while large CdS QDs were synthesized *via* the method developed by Peng *et al.*[51]

CdS-311, -366. CdO (2.2 mmol, 0.28 g), 5.7 mmol OA (1.8 g), and 8 g of ODE were heated at 260 °C for 20 min, then the solution was cooled to 30 °C. Meanwhile, a solution of 80 μL (360 μL for CdS-366) $(NH_4)_2S$ aqueous solution with 10 mL of OLA was prepared and stirred for 20 min. The $(NH_4)_2S$:OLA solution was injected at 30 °C and the solution was stirred for 1 h without heating. The CdS QDs were washed for one (for CdS-366) or two (for CdS-311) times using hexane and ethanol and dispersed in toluene.

CdS-404. CdO (1 mmol, 0.128 g), 3 mmol OA (0.942 g), and 15 g of ODE were heated at 260 °C for 20 min, then the temperature was set to 250 °C. A different S precursor was made for this and following CdS QD syntheses by dissolving S powder in ODE (0.5 M) at 130 °C. The S precursor (1 mL) was injected at 250 °C, and the solution was maintained at 240 °C for 20 min. The CdS QDs were washed twice using hexane and ethanol and dispersed in ODE.

CdS-425, -460. CdO (2 mmol, 0.256 g), 6 mmol OA (1.884 g), and 15 g of ODE were heated at 260 °C for 20 min, then the temperature was set to 265 °C. The S precursor (0.5 M, 1 mL, see CdS-404) was injected at 265 °C, and the solution was maintained at 250 °C. About 13 min later, additional S precursor was added dropwise until desired sizes were achieved. The CdS QDs were washed twice using hexane and ethanol and dispersed in ODE.

Synthesis of CdS and CdSe NRs. CdS and CdSe nanorods were synthesized following established methods[5,52] and were dispersed in ODE or toluene depending on the temperature for cation exchange (the higher temperatures used ODE).

Synthesis of PbS QDs from CdS QDs. *Pb Precursor.* OLA (5 mL) and $PbCl_2$ (1.5 mmol) were heated at 140 °C for 30 min until a white and turbid solution was achieved. Then, the solution was cooled or heated to a desired temperature for the injection of CdS QDs.

PbS-570. The Pb precursor was cooled down to 30 °C and 5 mL of toluene was added; then, the solution was further cooled to 5 °C using an ice bath. CdS-311 QDs (1 mL, 22 mg/mL) were injected swiftly, and a mixture of 5 mL of hexane and 3 mL of OA was injected immediately.

PbS-915. The Pb precursor was cooled down to 90 °C and 1 mL of CdS-366 in toluene (~30 mg/mL) was injected swiftly. Before the injection, the heating mantle was removed and the solution was allowed to cool down naturally after the injection. When the temperature reached 40 °C, 5 mL of hexane and 4 mL of OA were injected sequentially.

PbS-1032. The Pb precursor was cooled down to 120 °C, and 1 mL of CdS-366 in ODE (~58 mg/mL) was injected swiftly. Twenty seconds later, the reaction was quenched by a water bath, and 5 mL of hexane and 4 mL of OA were added at 70 and 40 °C respectively.

PbS-1318. The Pb precursor was heated to 190 °C, and 1 mL of CdS-425 in ODE (~36 mg/mL) was injected swiftly. Twenty seconds later, the reaction was quenched by a water bath, and 5 mL of hexane and 4 mL of OA were added at 70 and 40 °C respectively.

PbS-1952. The Pb precursor was heated to 190 °C, and 1 mL of CdS-460 in ODE (~20 mg/mL) was injected swiftly and temperature was maintained at 180 °C. Twenty minutes later, the reaction was quenched by a water bath, and 5 mL of hexane and 4 mL of OA were added at 70 and 40 °C, respectively.

The PbS QDs were washed 2−3 times using hexane and ethanol. There was some white precipitation in the washed QDs solutions, which can be removed by filtration.

Synthesis of CdSe and PbSe QDs. CdSe and PbSe QDs were synthesized following our previous method.[15]

Partial Cation Exchange. Larger CdS and CdSe QDs, and relatively low temperatures, were adopted to achieve partial exchange.

CdS/PbS. CdS-460 QDs were used, and the size is 5.7 nm estimated from the first exciton peak. The Pb precursor was cooled down to 90 °C, and 1 mL of CdS-460 in ODE (~20 mg/mL) was injected swiftly. The reaction flask was put in a water bath right after the injection, and 8 mL of hexane and 4 mL of OA were added at 70 and 40 °C, respectively.

CdS/PbS with Different Cd:Pb Ratio. CdS-458 QDs were used and the size is 5.6 nm estimated from the first exciton peak. The Pb precursor (10 mL OLA and 3 mmol $PbCl_2$) was set to a desired temperature and 5 mL of CdS-458 in toluene (~10 mg/mL) was injected swiftly. The reaction flask was put in a water bath right after the injection, and 10 mL of hexane was injected immediately. OA (8 mL) was added at 40 °C.

CdSe/PbSe. CdSe-629 QDs were used, and the size is 6.2 nm estimated from the first exciton peak. The Pb precursor was cooled down to 100 °C, and 1 mL of CdSe-629 in ODE (~50 mg/mL) was injected swiftly. The reaction flask was put in a water bath right after the injection, and 8 mL of hexane and 4 mL of OA were added at 70 and 40 °C, respectively.

Two-Step Synthesis of CdSe/PbSe. CdSe-580 QDs were used, and the size is 3.8 nm estimated from the first exciton peak. (I) The Pb precursor ($PbCl_2$, 5 ml OLA) was cooled down to 60 °C by removing the heat, and 1 mL of CdSe-580 in ODE (~130 mg/mL) was injected swiftly. Five seconds later, the reaction flask was put in a water bath, and 5 mL of hexane and 4 mL of OA were added. The product was washed two times using hexane and ethanol and dispersed in ODE as the seeds for the growth of PbSe. (II) PbO (0.125g), OA (0.5 g) and ODE (6g) were heated at 150 °C for 20 min, and 0.5 mL seeds in ODE (~20 mg/mL) was injected at 150 °C which was maintained. Fifteen seconds later, 0.25 mL of TOPSe (1 M) was injected. The reaction was allowed to proceed for 2 min, and then, the heat was removed to quench the growth. The product was washed two times using hexane and ethanol in a glovebox.

Cation Exchange Based on CdS and CdSe NRs. CdSe NRs in toluene (1 mL, ~50 mg/mL) were injected into Pb precursor at 150 °C, and 40 s later, the solution was cooled down using a water bath. CdS NRs in ODE and toluene (1 mL, 15 mg/mL) were injected into Pb precursor at 190 °C, and the temperature was maintained at 180 °C. Three minutes later, the solution was cooled down using a water bath. To monitor the evolution of the process in the cation exchange, CdSe NRs was injected at 80 °C and the temperature was maintained. At different intervals, aliquots of the reaction solution were withdrawn and dissolved

in hexane containing 10% (in volume) OA. The aliquot nanocrystals were washed and dissolved in TCE for measurements.

Cation Exchange Using ZnS QDs. ZnS QDs were synthesized following Robinson's method[50] without drying the sulfur precursor using molecular sieves. The ZnS QDs dispersed in ODE were injected into the Pb precursor at 195 °C, and the temperature was maintained for 90 s, followed by immersing the flask in a water bath. Hexane (5 mL) and OA (4 mL) were added at 80 and 40 °C, respectively.

Cation Exchange Using CdTe QDs. CdTe QDs (~3 nm) were synthesized *via* ref 53 but used tetradecylphosphonic acid (TDPA) instead of OA to yield spherical QDs. Briefly, 0.4 g of CdO, 1.87 g TDPA, and 63.5 g ODE were degassed with N_2 and heated to 260 °C until the solution turned clear. At this point, 2.2 mL of 0.75 M tributylphosphine telluride (TBP-Te) mixed with 10 mL of ODE were injected in the solution. The reaction was kept at temperature for 30 s (45 s for the larger ~3.6 nm QDs), taken off the heating mantle and allowed to cool naturally to 180 °C before immersing in a water bath. The CdTe QDs were washed three times by dissolution/precipitation with hexane and ethanol:isopropyl alcohol (1:1 ratio). Half of the reaction product was then dispersed in 2 mL of ODE and injected into the $PbCl_2$/OLA mixture at 180 °C. The temperature was maintained for 10 s, followed by immersing in a water bath. Hexane (10 mL) and OA (4 mL) were added at 70 and 30 °C, respectively. The resulting PbTe QDs were cleaned like the PbS QDs described above.

Study of Optical Stability of PbS QDs. The PbS QDs dispersed in hexane at a concentration of ~15 mg/mL were stored in a 4 mL vial in air with the vial loosely capped. Some hexane was added regularly to keep the amount of solvent constant. At different times, small amount of the QDs solution was dried and the QDs were redispersed in TCE for the absorption and PL QY measurements.

Characterization. Optical absorption spectra were collected using a Shimadzu UV-3600 spectrophotometer. TEM images were obtained using a FEI Technai G2 20 Twin microscope with a LaB_6 filament operated at 200 kV. XRD is performed on a Bruker D8 Discover diffractometer using Cu Kα radiation ($\lambda = 1.54$ Å). The PL QY was measured in a LabSphere integrating sphere, with excitation provided by monochromatic light selected from a xenon lamp passed through a monochromator (PTI). The emission and excitation spectra were measured with an InGaAs photodiode. The resulting InGaAs signal was amplified using a SRS SR530 lock-in amplifier. XPS data were obtained on a Physical Electronics 5600 photoemission system using monochromatic Al Kα radiation. For the measurement of PL spectrum of heterostructure, the emission in the range of 400−940 nm was collected by a silicon detector and the PL in the range of 940−2000 nm was detected by an InGaAs photodiode, and then the two segments were merged.

Conflict of Interest: The authors declare no competing financial interest.

Supporting Information Available: Absorption spectra of CdS starting nanocrystals, detailed synthetic conditions, XPS spectra of PbS QDs synthesized from CdS, TEM of partially exchanged CdSe QDs, PL spectra of starting CdS QDs, PL spectra of PbS/CdS Janus structures using CdS-443 as starting material, additional TEM of CdSe-PbSe heterostructures and CdTe QDs. The Supporting Information is available free of charge on the ACS Publications website at DOI: 10.1021/acsnano.5b01859.

Acknowledgment. This material is based upon work supported by the U.S. Department of Energy Office of Science, Office of Basic Energy Sciences. J.M.L, J.G., B.D.C. J.Z., and M.C.B acknowledge the Energy Frontier Research Centers program within the Center for Advanced Solar Photophysics, D.M.K. acknowledges support from the solar photochemistry program. DOE funding was provided to NREL through contract DE-AC36-08G028308. E.M.M. was supported an NREL Director's Postdoctoral Fellowship. J.Z. acknowledges partial support of the National Natural Science Foundation of China (No. 51302096) and the Fundamental Research Funds of Wuhan City (No. 2013060501010163).

REFERENCES AND NOTES

1. Son, D. H.; Hughes, S. M.; Yin, Y. D.; Alivisatos, A. P. Cation Exchange Reactions-in Ionic Nanocrystals. *Science* **2004**, *306*, 1009–1012.
2. Beberwyck, B. J.; Surendranath, Y.; Alivisatos, A. P. Cation Exchange: A Versatile Tool for Nanomaterials Synthesis. *J. Phys. Chem. C* **2013**, *117*, 19759–19770.
3. Gupta, S.; Kershaw, S. V.; Rogach, A. L. 25th Anniversary Article: Ion Exchange in Colloidal Nanocrystals. *Adv. Mater.* **2013**, *25*, 6923–6943.
4. Rivest, J. B.; Jain, P. K. Cation Exchange on the Nanoscale: An Emerging Technique for New Material Synthesis, Device Fabrication, and Chemical Sensing. *Chem. Soc. Rev.* **2013**, *42*, 89–96.
5. Robinson, R. D.; Sadtler, B.; Demchenko, D. O.; Erdonmez, C. K.; Wang, L. W.; Alivisatos, A. P. Spontaneous Superlattice Formation in Nanorods through Partial Cation Exchange. *Science* **2007**, *317*, 355–358.
6. Pietryga, J. M.; Werder, D. J.; Williams, D. J.; Casson, J. L.; Schaller, R. D.; Klimov, V. I.; Hollingsworth, J. A. Utilizing the Lability of Lead Selenide to Produce Heterostructured Nanocrystals with Bright, Stable Infrared Emission. *J. Am. Chem. Soc.* **2008**, *130*, 4879–4885.
7. Li, H.; Zanella, M.; Genovese, A.; Povia, M.; Falqui, A.; Giannini, C.; Manna, L. Sequential Cation Exchange in Nanocrystals: Preservation of Crystal Phase and Formation of Metastable Phases. *Nano Lett.* **2011**, *11*, 4964–4970.
8. Luther, J. M.; Zheng, H.; Sadtler, B.; Alivisatos, A. P. Synthesis of Pbs Nanorods and Other Ionic Nanocrystals of Complex Morphology by Sequential Cation Exchange Reactions. *J. Am. Chem. Soc.* **2009**, *131*, 16851–16857.
9. Murray, C. B.; Norris, D. J.; Bawendi, M. G. Synthesis and Characterization of Nearly Monodisperse CdE (E = S, Se, Te) Semiconductor Nanocrystallites. *J. Am. Chem. Soc.* **1993**, *115*, 8706–8715.
10. Yang, Y. A.; Wu, H.; Williams, K. R.; Cao, Y. C. Synthesis of Cdse and Cdte Nanocrystals without Precursor Injection. *Angew. Chem., Int. Ed.* **2005**, *44*, 6712–6715.
11. Beberwyck, B. J.; Alivisatos, A. P. Ion Exchange Synthesis of III-V Nanocrystals. *J. Am. Chem. Soc.* **2012**, *134*, 19977–19980.
12. Casavola, M.; van Huis, M. A.; Bals, S.; Lambert, K.; Hens, Z.; Vanmaekelbergh, D. Anisotropic Cation Exchange in Pbse/CdSe Core/Shell Nanocrystals of Different Geometry. *Chem. Mater.* **2012**, *24*, 294–302.
13. Lambert, K.; Geyter, B. D.; Moreels, I.; Hens, Z. Pbte|Cdte Core|Shell Particles by Cation Exchange, a HR-TEM Study. *Chem. Mater.* **2009**, *21*, 778–780.
14. Justo, Y.; Geiregat, P.; Hoecke, K. V.; Vanhaecke, F.; De Mello Donega, C.; Hens, Z. Optical Properties of Pbs/Cds Core/Shell Quantum Dots. *J. Phys. Chem. C* **2013**, *117*, 20171–20177.
15. Zhang, J.; Gao, J.; Church, C. P.; Miller, E. M.; Luther, J. M.; Klimov, V. I.; Beard, M. C. Pbse Quantum Dot Solar Cells with More Than 6% Efficiency Fabricated in Ambient Atmosphere. *Nano Lett.* **2014**, *14*, 6010–6015.
16. Wark, S. E.; Hsia, C. H.; Son, D. H. Effects of Ion Solvation and Volume Change of Reaction on the Equilibrium and Morphology in Cation-Exchange Reaction of Nanocrystals. *J. Am. Chem. Soc.* **2008**, *130*, 9550–9555.
17. Crisp, R. W.; Kroupa, D. M.; Marshall, A.; Zhang, J.; Beard, M. C.; Luther, J. M. Metal Halide Solid-State Surface Treatment for High Efficiency Pbs and PbSe QD Solar Cells. *Sci. Rep.* **2015**, *5*, 9945.
18. Hines, M. A.; Scholes, G. D. Colloidal PbS Nanocrystals with Size-Tunable near-Infrared Emission: Observation of Post-Synthesis Self-Narrowing of the Particle Size Distribution. *Adv. Mater.* **2003**, *15*, 1844–1849.
19. Lee, D. C.; Robel, I.; Pietryga, J. M.; Klimov, V. I. Infrared-Active Heterostructured Nanocrystals with Ultra Long Carrier Lifetimes. *J. Am. Chem. Soc.* **2010**, *132*, 9960–9962.
20. Nanayakkara, S. U.; Cohen, G.; Jiang, C. S.; Romero, M. J.; Maturova, K.; Al-Jassim, M.; van de Lagemaatt, J.; Rosenwaks, Y.; Luther, J. M. Built-in Potential and Charge Distribution within Single Heterostructured Nanorods

Measured by Scanning Kelvin Probe Microscopy. *Nano Lett.* **2013**, *13*, 1278–1284.
21. Malko, A. V.; Park, Y. S.; Sampat, S.; Galland, C.; Vela, J.; Chen, Y. F.; Hollingsworth, J. A.; Klimov, V. I.; Htoon, H. Pump-Intensity- and Shell-Thickness-Dependent Evolution of Photoluminescence Blinking in Individual Core/Shell Cdse/Cds Nanocrystals. *Nano Lett.* **2011**, *11*, 5213–5218.
22. Htoon, H.; Malko, A. V.; Bussian, D.; Vela, J.; Chen, Y.; Hollingsworth, J. A.; Klimov, V. I. Highly Emissive Multi-excitons in Steady-State Photoluminescence of Individual "Giant" CdSe/CdS Core/Shell Nanocrystals. *Nano Lett.* **2010**, *10*, 2401–2407.
23. Garcia-Santamaria, F.; Chen, Y. F.; Vela, J.; Schaller, R. D.; Hollingsworth, J. A.; Klimov, V. I. Suppressed Auger Recombination in "Giant" Nanocrystals Boosts Optical Gain Performance. *Nano Lett.* **2009**, *9*, 3482–3488.
24. Meinardi, F.; Colombo, A.; Velizhanin, K. A.; Simonutti, R.; Lorenzon, M.; Beverina, L.; Viswanatha, R.; Klimov, V. I.; Brovelli, S. Large-Area Luminescent Solar Concentrators Based on 'Stokes-Shift-Engineered' Nanocrystals in a Mass-Polymerized Pmma Matrix. *Nat. Photonics* **2014**, *8*, 392–399.
25. Lin, Q.; Makarov, N. S.; Koh, W.-k.; Velizhanin, K. A.; Cirloganu, C. M.; Luo, H.; Klimov, V. I.; Pietryga, J. M. Design and Synthesis of Heterostructured Quantum Dots with Dual Emission in the Visible and Infrared. *ACS Nano* **2015**, *9*, 539–547.
26. Cirloganu, C. M.; Padilha, L. A.; Lin, Q.; Makarov, N. S.; Velizhanin, K. A.; Luo, H.; Robel, I.; Pietryga, J. M.; Klimov, V. I. Enhanced Carrier Multiplication in Engineered Quasi-Type-II Quantum Dots. *Nat. Commun.* **2014**, *5*, 4148.
27. Beard, M. C.; Luther, J. M.; Semonin, O. E.; Nozik, A. J. Third Generation Photovoltaics Based on Multiple Exciton Generation in Quantum Confined Semiconductors. *Acc. Chem. Res.* **2013**, *46*, 1252–1260.
28. Kudera, S.; Carbone, L.; Casula, M. F.; Cingolani, R.; Falqui, A.; Snoeck, E.; Parak, W. J.; Manna, L. Selective Growth of Pbse on One or Both Tips of Colloidal Semiconductor Nanorods. *Nano Lett.* **2005**, *5*, 445–449.
29. Luther, J. M.; Zheng, H. M.; Sadtler, B.; Alivisatos, A. P. Synthesis of PbS Nanorods and Other Ionic Nanocrystals of Complex Morphology by Sequential Cation Exchange Reactions. *J. Am. Chem. Soc.* **2009**, *131*, 16851–16857.
30. Ha, D. H.; Caldwell, A. H.; Ward, M. J.; Honrao, S.; Mathew, K.; Hovden, R.; Koker, M. K. A.; Muller, D. A.; Hennig, R. G.; Robinson, R. D. Solid-Solid Phase Transformations Induced through Cation Exchange and Strain in 2D Heterostructured Copper Sulfide Nanocrystals. *Nano Lett.* **2014**, *14*, 7090–7099.
31. Pu, C. D.; Zhou, J. H.; Lai, R. C.; Niu, Y.; Nan, W. N.; Peng, X. G. Highly Reactive, Flexible yet Green Se Precursor for Metal Selenide Nanocrystals: Se-Octadecene Suspension (Se-Sus). *Nano Res.* **2013**, *6*, 652–670.
32. Yu, W. W.; Qu, L. H.; Guo, W. Z.; Peng, X. G. Experimental Determination of the Extinction Coefficient of Cdte, Cdse, and Cds Nanocrystals. *Chem. Mater.* **2003**, *15*, 2854–2860.
33. Moreels, I.; Lambert, K.; Smeets, D.; De Muynck, D.; Nollet, T.; Martins, J. C.; Vanhaecke, F.; Vantomme, A.; Delerue, C.; Allan, G.; et al. Size-Dependent Optical Properties of Colloidal PbS Quantum Dots. *ACS Nano* **2009**, *3*, 3023–3030.
34. Zhang, J.; Gao, J.; Miller, E. A.; Luther, J. M.; Beard, M. C. Diffusion Controlled Synthesis of PbS and PbSse Quantum Dots with in-Situ Halide Passivation for Quantum Dot Solar Cells. *ACS Nano* **2014**, *8*, 614–622.
35. Zhang, J.; Tolentino, J.; Smith, E. R.; Zhang, J.; Nozik, A. J.; Beard, M. C.; Law, M.; Johnson, J. C. Carrier Transport in PbS and PbSe QD Films Measured by Photoluminescence Quenching. *J. Phys. Chem. C* **2014**, *118*, 16228–16235.
36. Ip, A. H.; Thon, S. M.; Hoogland, S.; Voznyy, O.; Zhitomirsky, D.; Debnath, R.; Levina, L.; Rollny, L. R.; Carey, G. H.; Fischer, A.; et al. Hybrid Passivated Colloidal Quantum Dot Solids. *Nat. Nanotechnol.* **2012**, *7*, 577–582.
37. Thon, S. M.; Ip, A. H.; Voznyy, O.; Levina, L.; Kemp, K. W.; Carey, G. H.; Masala, S.; Sargent, E. H. Role of Bond Adaptability in the Passivation of Colloidal Quantum Dot Solids. *ACS Nano* **2013**, *7*, 7680–7688.
38. Smith, D. K.; Luther, J. M.; Semonin, O. E.; Nozik, A. J.; Beard, M. C. Tuning the Synthesis of Ternary Lead Chalcogenide Quantum Dots by Balancing Precursor Reactivity. *ACS Nano* **2011**, *5*, 183–190.
39. Murphy, J. E.; Beard, M. C.; Norman, A. G.; Ahrenkiel, S. P.; Johnson, J. C.; Yu, P.; Micic, O. I.; Ellingson, R. J.; Nozik, A. J. PbTe Colloidal Nanocrystals: Synthesis, Characterization, and Multiple Exciton Generation. *J. Am. Chem. Soc.* **2006**, *128*, 3241–3247.
40. Sadtler, B.; Demchenko, D. O.; Zheng, H.; Hughes, S. M.; Merkle, M. G.; Dahmen, U.; Wang, L. W.; Alivisatos, A. P. Selective Facet Reactivity During Cation Exchange in Cadmium Sulfide Nanorods. *J. Am. Chem. Soc.* **2009**, *131*, 5285–5293.
41. Peng, X.; Wickham, J.; Alivisatos, A. P. Kinetics of II-VI and III-V Colloidal Semiconductor Nanocrystal Growth: 'Focusing' of Size Distributions. *J. Am. Chem. Soc.* **1998**, *120*, 5343–5344.
42. Vigil, O.; Riech, I.; GarciaRocha, M.; ZelayaAngel, O. Characterization of Defect Levels in Chemically Deposited CdS Films in the Cubic-to-Hexagonal Phase Transition. *J. Vac. Sci. Technol., A* **1997**, *15*, 2282–2286.
43. Saunders, A. E.; Ghezelbash, A.; Sood, P.; Korgel, B. A. Synthesis of High Aspect Ratio Quantum-Size Cds Nanorods and Their Surface-Dependent Photoluminescence. *Langmuir* **2008**, *24*, 9043–9049.
44. Backhaus-Ricoult, M. Solid-State Reactivity at Heterophase Interfaces. *Annu. Rev. Mater. Res.* **2003**, *33*, 55–90.
45. Stevenson, D. A., Diffusion in the Chalcogenides of Zn, Cd and Pb. In *Atomic Diffusion in Semiconductors*; Shaw, D., Ed.; Springer: New York, 1973; pp 431−541.
46. Bansagi, T.; Secco, E. A.; Srivastava, O. K.; Martin, R. R. Kinetics of Hexagonal-Cubic Phase Transformation of Zinc Sulfide in Vacuo, in Zinc Vapor, and in Sulfur Vapor. *Can. J. Chem.* **1968**, *46*, 2881–2886.
47. Justo, Y.; Goris, B.; Kamal, J. S.; Geiregat, P.; Bals, S.; Hens, Z. Multiple Dot-in-Rod PbS/CdS Heterostructures with High Photoluminescence Quantum Yield in the Near-Infrared. *J. Am. Chem. Soc.* **2012**, *134*, 5484–5487.
48. Bals, S.; Casavola, M.; van Huis, M. A.; Van Aert, S.; Batenburg, K. J.; Van Tendeloo, G.; Vanmaekelbergh, D. Three-Dimensional Atomic Imaging of Colloidal Core-Shell Nanocrystals. *Nano Lett.* **2011**, *11*, 3420–3424.
49. Yalcin, A. O.; Fan, Z. C.; Goris, B.; Li, W. F.; Koster, R. S.; Fang, C. M.; van Blaaderen, A.; Casavola, M.; Tichelaar, F. D.; Bals, S.; et al. Atomic Resolution Monitoring of Cation Exchange in CdSe-PbSe Heteronanocrystals During Epitaxial Solid-Solid--Vapor Growth. *Nano Lett.* **2014**, *14*, 3661–3667.
50. Zhang, H. T.; Hyun, B. R.; Wise, F. W.; Robinson, R. D. A Generic Method for Rational Scalable Synthesis of Monodisperse Metal Sulfide Nanocrystals. *Nano Lett.* **2012**, *12*, 5856–5860.
51. Yu, W. W.; Peng, X. G. Formation of High-Quality CdS and Other II-VI Semiconductor Nanocrystals in Noncoordinating Solvents: Tunable Reactivity of Monomers. *Angew. Chem., Int. Ed.* **2002**, *41*, 2368–2371.
52. Gur, I.; Fromer, N. A.; Geier, M. L.; Alivisatos, A. P. Air-Stable All-Inorganic Nanocrystal Solar Cells Processed from Solution. *Science* **2005**, *310*, 462–465.
53. Crisp, R. W.; Panthani, M. G.; Rance, W. L.; Duenow, J. N.; Parilla, P. A.; Callahan, R.; Dabney, M. S.; Berry, J. J.; Talapin, D. V.; Luther, J. M. Nanocrystal Grain Growth and Device Architectures for High-Efficiency Cdte Ink-Based Photovoltaics. *ACS Nano* **2014**, *8*, 9063–9072.